Energ. Ecol. Environ. (2021) 6(1):55–68
https://doi.org/10.1007/s40974-020-00153-7

ORIGINAL ARTICLE

Co-fired anode-supported solid oxide fuel cell for internal reforming of hydrocarbon fuel

S. Senthil Kumar[1] · **Vikram Jayaram**[2] · **S. T. Aruna**[1]

[1] Surface Engineering Division, CSIR-National Aerospace Laboratories, Bangalore, India
[2] Materials Engineering Department, Indian Institute of Science, Bangalore, India

Received: 15 October 2019 / Revised: 4 March 2020 / Accepted: 5 March 2020 / Published online: 18 March 2020

Abstract Hydrocarbon-based solid oxide fuel cell (SOFC) is being projected as one of the possible alternatives to conventional internal combustion engines. However, the conventional Ni–YSZ anode is prone to carburization in the presence of hydrocarbon fuels. In the present study, an optimized Ni–Cu-based anode composition ($Ni_{0.9}$–$Cu_{0.1}$–$YSZ_{0.95}$–$GDC_{0.05}$) has been evolved based on accelerated carburization studies and phase analysis by X-ray diffractometry and X-ray photoelectron spectroscopy. The electrochemical parameters have been derived for the optimized anode composition, and its exchange current density is estimated to be 76.3 mA cm^{-2} at 780 °C. The main advantage of the optimized anode is its suitability for co-firing with the electrolyte. Using the optimized anode composition, anode-supported SOFC single cells (ASCs) have been fabricated and their electrical and electrochemical performances have been evaluated and compared with conventional ASC. The anode-supported co-cast SOFC with the optimized anode composition exhibits a power density of 436 mW cm^{-2} at 850 °C and 0.5 V with methane as fuel.

Electronic supplementary material The online version of this article (https://doi.org/10.1007/s40974-020-00153-7) contains supplementary material, which is available to authorized users.

✉ S. T. Aruna
aruna_reddy@nal.res.in

Graphic abstract

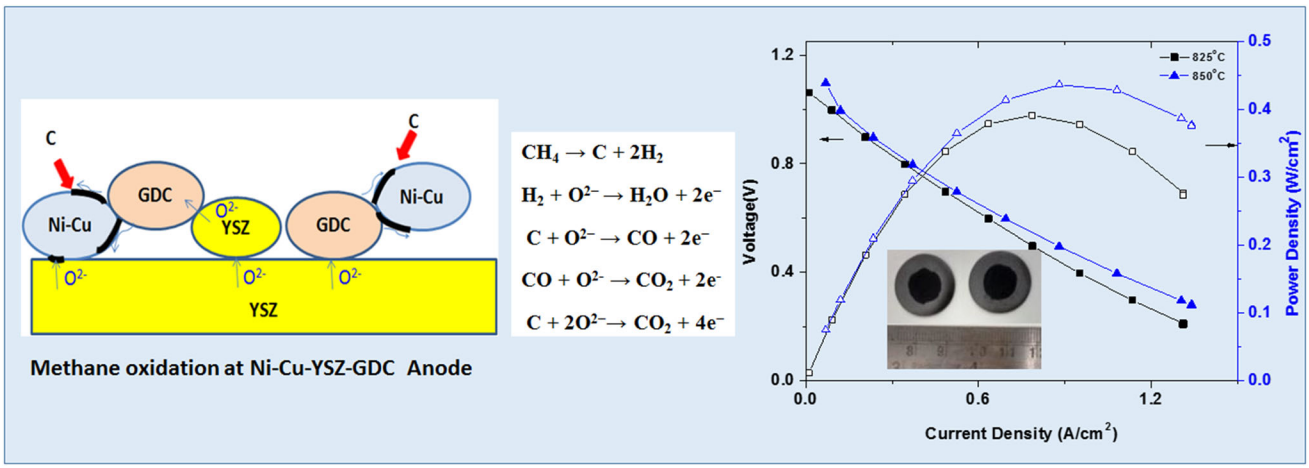

Keywords SOFC anode · Carburization · Methane · Tape-casting · Co-firing

1 Introduction

Direct internal reforming in solid oxide fuel cell (SOFC) is the subject of intense research in recent years. There have been attempts to utilize hydrocarbons directly in the fuel cells to avoid external reforming. As SOFCs are being operated at a high temperature, the direct internal reforming of hydrocarbon fuel can be accommodated in the anode itself. However, the present state-of-the-art anode, Ni–YSZ, is much prone to carburization in carbonaceous fuels. Being a potential catalyst for the carbon nanotubes (CNT)/graphene synthesis, the Ni grains in anode facilitate carbon fiber growth and result in metal dusting (Chun and Ramanarayanan 2007). This would eventually disintegrate the entire anode resulting in cell failure. So far, numerous anode compositions have been investigated.

New anode developments are mostly focused on ceramic oxides and bimetallic anode systems (Zhao et al. 2019; Sarno et al. 2018; Neofytidis et al. 2018). Lanthanum strontium chromium manganite (LSCM), lanthanum strontium titanate (LST) and yttrium strontium titanate (YST) are the commonly explored ceramic anodes. But ceramic oxide anodes exhibit moderate catalytic activity. Kim et al. (2008, 2009) observed enhanced performance with the addition of Pd and CeO_2 on to LSCM anode. Ma et al. (2010, 2011a, b) investigated YST anode catalyst in various configurations and reported improved performance on YST-infiltrated NiO anode. Kim et al. (2009) have also highlighted the role of Pt contact layer in enhancing the performance of the oxide anodes. On the contrary, metals have good electronic conductivity and metals such as Ni, Co, Ru, Ir and Rh show better catalytic activity for hydrogen oxidation reaction in the typical operating condition of SOFC (Ingram and Linic 2009). Unfortunately, Ni and Co are susceptible to carburization and Ru, Ir and Rh are not economically viable.

Therefore, in recent years, a large number of bimetallic anode systems have been developed. Among them, bimetallic alloys such as Ni–Fe and Ni-Cu are found to be promising (Lu et al. 2009; Kim et al. 2002). As Fe does not catalyze Boudouard reaction, it has been considered for anode catalysis below 700 °C. However, partial oxidation behavior of hydrocarbon fuel and choking of fuel lines are the major issues at low temperature, whereas at high temperature, Ni has the advantage over Ni–Fe alloy with regard to carbon diffusivity. Conversely, Ni–Cu alloys are found to perform impressively in the temperature regime of around 800 °C. Cu is known to control carbon deposition due to its inability to catalyze the formation of the C–C bond. As Boudouard and methane cracking reactions are suppressed around 800 °C, it could be the right temperature to handle methane for a bimetallic cermet like Ni–Cu–YSZ. Kim et al. reported 4–5 times increase with respect to the initial performance of Ni–Cu–YSZ system over the period of 500 h of operation (Gupta et al. 2006). Gorte et al. reported reasonably good performance (0.09 W cm^{-2} with CH_4 @ 700 °C) for the Cu–CeO_2–YSZ system at 700 °C. The addition of CeO_2 improved the anode catalysis, and partial oxidation behavior at these temperature regimes was observed (Gorte et al. 2002; Park et al. 2000). However, most of the developed compositions to date have failed to meet the stringent co-sintering fabrication conditions of anode-supported SOFC (1350–1400 °C). In copper-rich anodes, during high-temperature sintering, Cu segregates are formed in the anode, which in turn results in reduced catalytic activity. The optimization of Cu content

is required to inherit both carbon tolerance and thermal stability qualities in these anode systems. Presently, most of the developed Ni-Cu anode systems are utilized for electrolyte-supported cells in which the anodes are heat treated at a relatively low temperature (1100 °C). Thus, the established anode compositions have failed to tap the benefit of anode-supported SOFC where the electrolyte thickness can be as low as 10 μm. In order to realize Cu based anode composition in anode-supported SOFC, tedious leaching and infiltration techniques have been used (Gorte et al. 2002; Fuerte et al. 2011; Kaur and Basu 2013; Camacho and Vivas 2009). Moreover, the infiltrated ceria catalyst in the porous YSZ matrix undergoes severe deactivation in the presence of hydrocarbon fuel (Kim et al. 2007). Thus, it was evident from the above reports that Ni–Cu-based anode compositions were mostly demonstrated for electrolyte-supported SOFC. However, utilizing those compositions in anode supported configuration will pave the way to improve the performance. So there is need to tailor the Ni–Cu-based anode composition for anode-supported SOFC, which involves high-temperature manufacturing process. The merit of the fabrication process is mainly decided upon the scalability and performance of the product it yields. In this context, tape-casting is the industrial scalable process and the co-firing process is considered as the most versatile and economical process. So, the main aim of this work was to formulate optimum anode composition (devoid of noble metals) with carbon tolerance and suitable for the standard well-established co-firing fabrication conditions.

In the present work, Ni–Cu–YSZ with GDC (gadolinia-doped ceria)-based anode system was optimized to match the stringent fabrication and operating conditions of anode-supported SOFC. Carbon-resistant property of the anode composition was identified by an accelerated carburization study. The anode composition with thermal and redox stability was fabricated in the form of electrolyte-supported cell to establish its electrochemical parameters such as electrode impedance and exchange current density. The optimized anode composition was fabricated in the form of anode-supported cells by tape-casting co-firing process. The fabrication of thermally sensitive Ni–Cu anode compositions by the co-firing process is least explored to date. As a maiden attempt, $Ni_{0.9}$–$Cu_{0.1}$–$YSZ_{0.95}$–$GDC_{0.05}$ anode-supported SOFC has been fabricated by tape-casting technique followed by the co-firing. As the fabrication methods also influence the electrocatalytic activity of the anode, the electrochemical properties of the fabricated $Ni_{0.9}$–$Cu_{0.1}$–$YSZ_{0.95}$–$GDC_{0.05}$ anode-supported cell were established. Further, anode-supported SOFC has been fabricated with bilayer consisting of co-casted YSZ electrolyte and $Ni_{0.9}$–$Cu_{0.1}$–$YSZ_{0.95}$–$GDC_{0.05}$ anode. The co-casting process was expected to increase the electrochemical performance due to intact anode–electrolyte interface. Thus, the work demonstrates the possibility to utilize Cu in a high-temperature fabrication process so as to evolve a hydrocarbon compatible SOFC with better performance.

2 Experimental

The anode powder, anode tapes, YSZ tapes and single cells were prepared using nickel oxide (NiO) (Inframat, USA), copper oxide (CuO) (Sigma-Aldrich), 8 mol% yttria-stabilized zirconia (8YSZ) (Tosho, Japan) and lanthanum strontium manganite ($La_{0.65}Sr_{0.3}MnO_3$, LSM) (Inframat Advanced Materials, USA). Solution combustion method was used for the synthesis of 20 mol% gadolinia-doped ceria (GDC) nanopowder using Gd_2O_3 (China Rare Earths), ceric ammonium nitrate (Mincometsal, India), glycine (Merck) and nitric acid (Merck). For the solution combustion synthesis, oxidizer-to-fuel ratio was maintained as unity (Patil et al. 2002). Tape-casting slurry was prepared by mixing anode powder with ethanol (Merck), toluene (Merck), benzyl butyl phthalate (Sigma-Aldrich) and polyvinyl butyral (Sigma-Aldrich). Screen-printing ink was prepared by mixing the anode powder with ethyl cellulose binder (S.D. Fine) and terpineol (Himedia).

Suitable anode composite material for hydrocarbon compatible SOFC was selected based on the accelerated carburization studies. Accordingly, systematic carburization studies were carried out on the anode system $Ni_{(1-x)}$–Cu_x–$YSZ_{(1-y)}$–GDC_y (where weight fraction $x = 0.1$–0.9 and $y = 0.05$). The results of the carburization study are relative rather than absolute. The amount of carbon deposited on the modified anode was quantified with respect to standard Ni–YSZ composition. The carbon deposition was quantified by measuring the difference in weight of the compositions before and after deposition. In the present study, the weight ratio of metal/oxide in anode composition was 57:43. All the above compositions were reduced at 950 °C for 2 h in $4Ar/1H_2$ atmosphere. The reduced compositions were then carburized in a custom-built CVD reactor under accelerated carburization conditions by loading different new anode compositions along with the standard Ni–YSZ composition. Followed by reduction, the carburization was carried out at 950 °C for about 1 h by passing ethanol (Gupta et al. 2006) into the reaction chamber at the rate of 1 ml min^{-1}. Thus, anode compositions were then subjected to phase analysis.

Phase analysis of the anode powders and YSZ–GDC solid solution was done using XRD (Bruker D-8 Advance X-ray diffractometer). XRD analysis was carried out between 2θ values of 10°–90° at the scan rate of 2° min^{-1} to check phase stability. X-ray photoelectron spectroscopy

(XPS) was used to study the redox stability of the anode system before and after carburization. Accordingly, SPECS Surface Nanoanalysis X-ray photoelectron spectrometer was used. The anode composition, which had shown resistance to carbon deposition and redox stable, was identified and subjected to electrical and electrochemical characterizations.

The electrical conductivity of the developed anode compositions (1-mm-thick pellets sintered at 1275–1375 °C) was measured using Vander Pauw (DC 4-probe) method with 100 mA current source (Keithley 6221) and nanovoltmeter (Keithley). Samples of anode composites were prepared, sintered and reduced in the hydrogen atmosphere. Reduction was done at 750 °C in air at the rate of 2 °C min^{-1} followed by reduction in 20:80 H_2–N_2 mixture gas for 4 h. The conductivities were measured at different temperatures (25–700 °C). Thus, selected potential anode composition was fabricated into various SOFC configurations, viz. electrolyte-supported SOFC (ESC); standard anode supported SOFC (ASC) and ASC with bilayer electrolyte–anode tape (co-casted).

In order to establish detailed electrochemical parameters, ESC was fabricated using 2 mm uniaxially pressed and sintered electrolyte. LSM cathode and anode ink was screen printed on the electrolyte. The anode ink was made using $Ni_{0.9}$–$Cu_{0.1}$–$YSZ_{0.95}$–$GDC_{0.05}$ anode cermet and fired at 1300 °C for 2 h. Electrochemical characterization on ESC was done to establish the anode impedance and anode exchange current density using dry H_2 as fuel. Anode impedance data were obtained by three-electrode technique with the anode as the working electrode (WE), the anode side reference electrode (RE) and the cathode as the counter electrode (CE) (Prakash et al. 2017). The position of WE, RE and CE is shown in Fig. S1. The total cell impedance was measured between two electrodes in which the cathode acted as the working electrode and the anode as the counter and reference electrode. CH electrochemical analyzer (CHI 604 2D electrochemical work station) controlled by CHI604D software was used for impedance measurements. The experiment was conducted under the OCV condition, 1 MHz to 0.1 Hz frequency range with a voltage of 10 mV amplitude. The exchange current density (i_o) was measured similar to earlier report (Zhou et al. 2011) using the above electrochemical analyzer. Accordingly, step voltage polarization measurement was carried out with positive overpotential and with voltage steps of 0.01 V s^{-1} in the voltage range of 0 V to OCV. The exchange current density was obtained from the Tafel intercept, i.e., log(i) axis intercept of overpotential versus log(i) plot.

The anode-supported SOFC (ASC) with an active area of 1 cm^2 was fabricated by the standard tape-casting followed by sintering and screen-printing processes. Green ceramic tapes comprising $Ni_{0.9}$–$Cu_{0.1}$–$YSZ_{0.95}$–$GDC_{0.05}$ anode cermet powders were prepared and laminated along with a thin YSZ electrolyte green tape. The green laminate was co-fired at 1350 °C for 6 h. The prepared half-cell was screen printed with LSM cathode ink and again fired at 1100 °C for 2 h. Thus, fabricated anode supported cell (ASC) consisted of 50 μm cathode, 15 μm electrolyte and 1 mm anode, respectively, and is hereinafter termed as $Ni_{0.9}$–$Cu_{0.1}$–$YSZ_{0.95}$–$GDC_{0.05}$ anode-supported SOFC with laminated layers of electrolyte and anode tapes (ANCZGL). The performance of the cell varies with the fabrication and test conditions. In order to overcome this ambiguity, a standard Ni–YSZ anode-supported SOFC single cell (ANZL) was also fabricated by the aforementioned procedure and its performance was compared with ANCZGL. In order to improve the interaction between electrolyte and anode, ASC was also prepared by co-casting of YSZ electrolyte on $Ni_{0.9}$–$Cu_{0.1}$–$YSZ_{0.95}$–$GDC_{0.05}$ anode tape. Thus, prepared electrolyte–anode bilayered tape was utilized for the fabrication of anode-supported cell and is termed as $Ni_{0.9}$–$Cu_{0.1}$–$YSZ_{0.95}$–$GDC_{0.05}$ anode-supported SOFC with co-casted bilayered tape (ANCZGC).

For electrochemical characterizations, the button cells of ESC, ANCZGL, ANCZGC and ANZL with 1 cm^2 were mounted on a test bench using a suitable ceramic sealant (Ceramabond 552, Aremco). The SOFC test bench (Fuel Cell technologies, USA) was heated to 800 °C at the rate 2 °C min^{-1} in air followed by 4 h reduction in 20:80 H_2–N_2, and the performance studies were conducted in dry H_2 and methane fuels on 1 cm^2 button cells (Park et al. 2000). The fuel flow rate and the oxygen flow rate were maintained at 50 and 100 sccm, respectively. Since the cells were tested with ceramabond sealant, it was difficult to recover the cells after experiments. At least 2–3 cells were used in each configuration to complete the entire set of experiments. To identify similar performing cells, performance in H_2 at 800 °C was used. The measurements were recorded after 3 h of equilibration time at each temperature.

3 Results and discussion

A systematic investigation on Ni–Cu–YSZ–GDC system was carried out to identify a suitable composition that can withstand both fabrication conditions and performance criteria of SOFC. Cu addition to Ni is known to reduce the carbon deposition but has serious implication on the thermal stability (Gross et al. 2007; Eric and Timu 1979) due to the lower melting point in comparison with pure Ni. As the co-firing process demands better thermal stability, a perfect balance has to be made between these requirements.

3.1 Effect of Cu addition

The carbon deposition is known to decrease drastically with increasing Cu content, and hence, Cu has been used liberally in low-temperature fabrication processes (Kim et al. 2002). However, those compositions cannot be fabricated as ASC by the co-firing technique. In the present work, accelerated carburization studies were carried out on Ni–Cu–YSZ system. The effect of Cu addition to the anode cermet (Ni–YSZ) on carbon deposition is shown in Fig. 1. Ni_{1-x}–Cu_x–YSZ ($x = 0.5$) anode composition showed a reduction in the carbon deposition to one-fifth of the conventional Ni–YSZ anode. Further increase in Cu did not reduce the carburization. Cu is known to suppress the carburization due to the fact that the filled d-orbital of Cu does not catalyze the C–C bond formation (Ingram and Linic 2009; Rodriguez et al. 1993). Unfortunately, Cu is also a poor catalyst for C–H scission. So, the electrochemical oxidation of hydrocarbon fuel also reduces with the addition of Cu. On the other hand, higher Cu content has serious implications on the performance of the anode due to the formation of low melting phases. Therefore, it is essential to optimize the Cu content in anode cermet to enable it to withstand the fabrication and operating conditions of SOFC.

The XRD patterns of Ni_{1-x}–Cu_x–YSZ anode cermet compositions are shown in Fig. 2. There was no additional phase formation as Ni–Cu forms an isomorphous substitutional solid solution (Fig. 2b). The gradual shifting of XRD peaks toward lower 2θ values with the addition of Cu may be attributed to the higher ionic radius of Cu atom (0.72 Å) in comparison with Ni (0.69 Å). However, the anode compositions with higher Cu content, i.e., $x = 0.5$ and above, exhibited minor secondary phase like Cu_2O (Fig. 2c). This may be because of the high fabrication

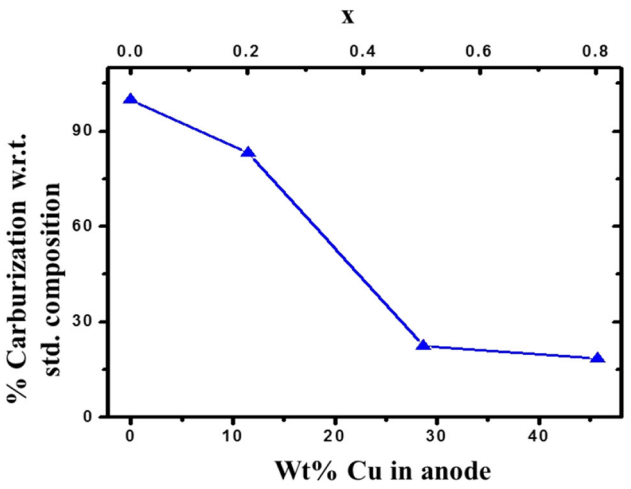

Fig. 1 Effect of Cu addition in Ni_{1-x}–Cu_x–YSZ on the carburization

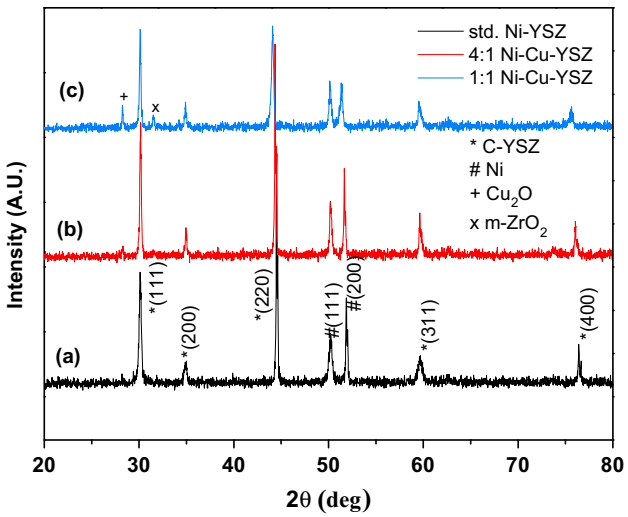

Fig. 2 XRD patterns of (a) Ni–YSZ, (b) 4Ni/1Cu–YSZ and (c) 1Ni/1Cu–YSZ sintered at 1375 °C for 6 h

temperature. Though Ni and Cu form a solid solution at all compositions, NiO and CuO form secondary CuO phase around 20 wt% of CuO (Eric and Timu 1979). So, while fabricating in the form of 50NiO/50CuO, there may be the possibility of segregation of secondary copper oxide phase at the surface. Even in reduced conditions, it can persist as segregated Cu metal, and during cooling of the anode, traces of segregated Cu_2O can reappear. In any case, $\geq$ 20 wt% Cu content does not support the proposed co-sintering fabrication procedure due to melting issues above 1200 °C. Thus, based on the present carburization studies and also on published the literature, 10 wt% Cu in metallic phase was reasonably adequate to suppress the carburization (Li et al. 2015; Zhao et al. 2011; Wang et al. 2008).

3.2 Effect of GDC addition

In general, high ionic conductivity is believed to improve the durability of the anode in hydrocarbon fuel (Sumi et al. 2015; Shiratori et al. 2008). Cubic fluorite-structured oxides are known to possess better ionic conductivity due to their lattice symmetry. Rare-earth-based fluorite compounds further improve the catalytic activity. Rare-earth oxides are well recognized for their steam reforming and methane oxidation ability. Among the rare-earth oxides, CeO_2 gives reasonably high H_2 yield and has a tendency to suppress carbon deposit (Wu et al. 2007). CeO_2 is a mixed ionic–electronic conductor, which transports electrons and oxygen ions via n-type small polaron hopping and oxygen vacancies, respectively. Doping ceria with gadolinia can further increase the ionic conductivity due to the increase in oxygen vacancies (Rupp et al. 2007). This results in the improvement of the overall electrochemical performance of the anode. Based on these facts, gadolinia-doped ceria

(GDC) was incorporated into the ceramic (YSZ) part of the anode composite. GDC is also considered as a potential candidate to reduce the local temperature gradient via controlled steam reforming reaction due to the reversible transformation between Ce^{4+} and Ce^{3+} (Cabrera et al. 2004). Thus, the presence of Gd^{3+}/Ce^{3+} in the FCC lattice of Ce^{4+} atoms fosters the catalytic activity for oxidation (Palaniyandi et al. 2006). The possible mechanistic model for methane oxidation reaction is shown in Fig. S2.

Accordingly, in the present anode system, YSZ–GDC solid solution with minor GDC phase in YSZ matrix has been employed. In addition, this can effectively eliminate the catalyst deactivation which is common in anodes fabricated by infiltration process (Kim et al. 2007). Though the formation of YSZ–GDC solid solution mitigates deactivation of the catalyst, the solid-state reaction between YSZ and GDC during the preparation of the anode can result in the formation of low ionic conducting phases, which separate the ionic conduction route between the dispersed GDC and YSZ matrix (Rührup et al. 2006; Constantin et al. 2012; Mishima et al. 1998). Hence, the concentration of GDC was restricted in the range of 2–5 wt% of total anode composition (Fig. S3).

In addition, the electrical conductivity of the YSZ–GDC solid solution was measured and compared with pure YSZ and GDC (Table 1). There was no appreciable change in the electrical conductivity of YSZ–GDC solid solution, which confirmed the absence of adverse reaction in the 7:1 YSZ–GDC composition. Although there was no change in the conductivity, it is believed that the redox behavior of Ce^{4+} ions improves the catalytic activity for the electrochemical oxidation of deposited carbon on the anode composite (Muccillo et al. 2008).

The carburization studies (Fig. S4) showed that $Ni_{0.9}$–$Cu_{0.1}$–$YSZ_{0.95}$–$GDC_{0.05}$ composition is reasonably good in controlling carburization (50% reduction) and besides, the composition exhibited better thermal stability during fabrication at 1375 °C. This was further confirmed by comparing the electrochemical performance of $Ni_{0.9}$–$Cu_{0.1}$–$YSZ_{0.95}$–$GDC_{0.05}$ anode with standard Ni–YSZ anode system.

Table 1 Electrical conductivity of oxide phases

Compound	Electrical conductivity (S cm^{-1}) at 650 °C
YSZ	0.0034
GDC	0.0078
YSZ–GDC (7:1)	0.0032

3.3 Electrical conductivity

Figure 3 shows the plots of electrical conductivity with respect to temperature for the developed anodes and standard Ni–YSZ. The $Ni_{0.8}$–$Cu_{0.2}$–$YSZ_{0.95}$–$GDC_{0.05}$ was not thermally stable at the typical sintering temperature (1375 °C) of anode-supported SOFC. So, it was sintered at a relatively lower temperature (1275 °C). All the cermet showed metallic behavior, i.e., conductivity decreases with increase in temperature. It was evident from the conductivity data that even for standard Ni–YSZ, the conductivity was higher in 1275 °C sintered sample than the 1375 °C sintered sample. At higher temperatures, Ni agglomeration is higher, and hence, it is expected to deter the conductivity to some extent. The electronic conductivity of anode cermet can be given as (Simwonis et al. 2000)

$$\sigma_{\text{cermet}} = \sigma_{\text{Ni}} V_{\text{Ni}} C_{\text{Ni}} \quad (1)$$

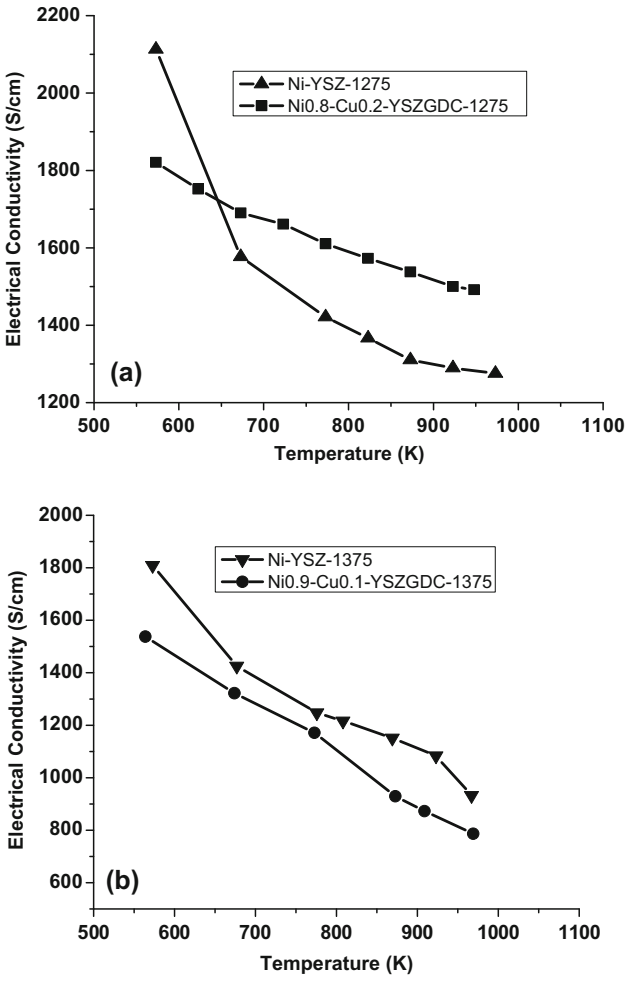

Fig. 3 Effect of temperature on electrical conductivity of **a** filled triangle Ni–YSZ and filled square $Ni_{0.8}$–$Cu_{0.2}$–$YSZ_{0.95}$–$GDC_{0.05}$ sintered at 1275 °C and **b** filled inverted triangle Ni–YSZ and filled circle $Ni_{0.9}$–$Cu_{0.1}$–$YSZ_{0.95}$–$GDC_{0.05}$ anodes sintered at 1375 °C

where σ_{cermet} is the electronic conductivity of cermet, σ_{Ni} is the electronic conductivity of Ni, V_{Ni} is the volume fraction of the nickel, and C_{Ni} is the contact area fraction of the nickel phase.

The increase in particle size of Ni ensemble reduces the C_{Ni}, and the electrical conductivity decreases due to the reduction in electrical conduction path. The conductivity trend of 1275 °C sintered cermets showed that the decrease in conductivity of $Ni_{0.8}$–$Cu_{0.2}$–$YSZ_{0.95}$–$GDC_{0.05}$ with temperature was low in comparison with Ni–YSZ anode. The possible reason may be the formation of Cu-rich phase at the interface of nickel and YSZ grains in $Ni_{0.8}$–$Cu_{0.2}$–$YSZ_{0.95}$–$GDC_{0.05}$ anode composition. This segregated phase would have established a second conduction path to sustain the conductivity. Hence, the $Ni_{0.8}$–$Cu_{0.2}$–$YSZ0_{.95}$–$GDC_{0.05}$ anode conductivity was marginally higher than that of the standard Ni-YSZ.

The conductivity trend of 1375 °C sintered cermets showed that the slope of conductivity vs temperature was almost same for $Ni_{0.9}Cu_{0.1}YSZ_{0.95}$–$GDC_{0.05}$ and Ni–YSZ. As expected, $Ni_{0.9}$–$Cu_{0.1}$–$YSZ0_{.95}$–$GDC_{0.05}$ exhibited lower electrical conductivity compared to Ni–YSZ due to the effect of alloying.

As far as the electrolyte-supported cells are concerned, a sintering temperature of 1275 °C is sufficient. Nevertheless, the processing of anode compositions at 1375 °C is mandatory for anode-supported cells. From the phase diagram of NiO–CuO, it is evident that 9:1 NiO–CuO solid solution is not supposed to yield any secondary phases during firing at 1375 °C. Therefore, $Ni_{0.9}$–$Cu_{0.1}$–YSZ0.95–$GDC_{0.05}$ composition was preferred over $Ni_{0.8}$–$Cu_{0.2}$–$YSZ_{0.95}$–$GDC_{0.05}$ for anode-supported cell fabrication process. Nonetheless, the electrical conductivity of both compositions was found to be suitable for SOFC application.

3.4 XPS analysis

Anodes of SOFC undergo various redox processes during SOFC fabrication and operating conditions. For instance, the metal oxide–ceramic composite anode would be reduced to metal–ceramic during SOFC operating condition. Further, there is a possibility of oxidizing back to original oxide during cooling due to minor air leakage or during an emergency shutdown. Moreover, the tendency of anode metal catalyst to form carbide in the presence of hydrocarbon fuel can result in metal dusting. Even a slight change in the microstructure or crystal structure in this process would initiate anode failure. There are many reports, which capture the presence of Ni_3C during carbon filament formation (Kharlamova 2017; Bayer et al. 2016; Rao et al. 2014; Yu et al. 2019; Sun et al. 2019). Esconjauregui et al. (2009) have reported such intermediate Ni_3C phase with ex situ XRD studies. So, XPS study was carried out to identify such a phase and also study the redox stability of the developed anode. The XPS spectra of the as-prepared, carburized and re-oxidized anodes were generated, and the peaks were identified. There was no visible change in the spectra of as-prepared and re-oxidized samples (Fig. 4a). As expected, the carbon peak intensity was enhanced in the carburized sample. The Ni_3C peak was not observed at 283.0 eV. Also, Ni_2C peak at 283.2 eV that appears due to monolayer reconstruction on Ni surface is absent (Bayer et al. 2016). Thus, it was evident that there was no nickel carbide formation during carburization (Fig. 4b).

Similarly, the valency of Cu was investigated to check any deviations in the oxidation states (Fig. 4c). No visible peak shift was detected between the as-prepared and the re-oxidized samples. The suppression of the satellite peak of Cu in the carburized sample indicated the reduction in copper oxide to Cu metal. In the re-oxidized sample, Cu metal was back to the original Cu^{2+} state. It confirmed the absence of any disruptive phase transformation. Also, there was no deviation in the valency of Ni. Thus, the redox stability of the developed $Ni_{0.9}$–$Cu_{0.1}$–$YSZ_{0.95}$–$GDC_{0.05}$ anode was found to be good.

3.5 Microstructure of anodes

Figure 5 shows the FESEM image of anode-supported SOFC (ANCZGL). The electrolyte layer was highly dense without any pores. The thickness of the electrolyte was 10–12 μm. Thus, the YSZ electrolyte was sufficiently thin and dense to permit oxygen ion conduction while restricting the molecular diffusion of oxygen. Further, the anode–electrolyte interface was found to be intact without any delamination and there were no signs of interface reactivity, which ensured low interfacial resistance.

The anode was found to be sufficiently porous. The grain size was in the range of 2–3 μm. More interestingly, fine pores of 100 nm were generated due to the reduction in the metal oxide solid solution. These pores were uniformly distributed along with larger pores of 2 μm size, and such architecture facilitates the formation of TPB with an extended active zone, which will improve the catalytic activity of the anode. The anode microstructure after performing in CH_4 fuel for 48 h is shown in Fig. 5d. No carbon fiber was seen, whereas standard Ni–YSZ cermet tends to grow carbon fiber within 2 h (Yu et al. 2019). The microstructure was porous, and there was no evidence of metal segregation.

EDAX analysis on the Ni–Cu metallic grain (Fig. S5) was carried out. The composition closely matches the expected weight ratio of 9:1 Ni–Cu. In order to examine Cu

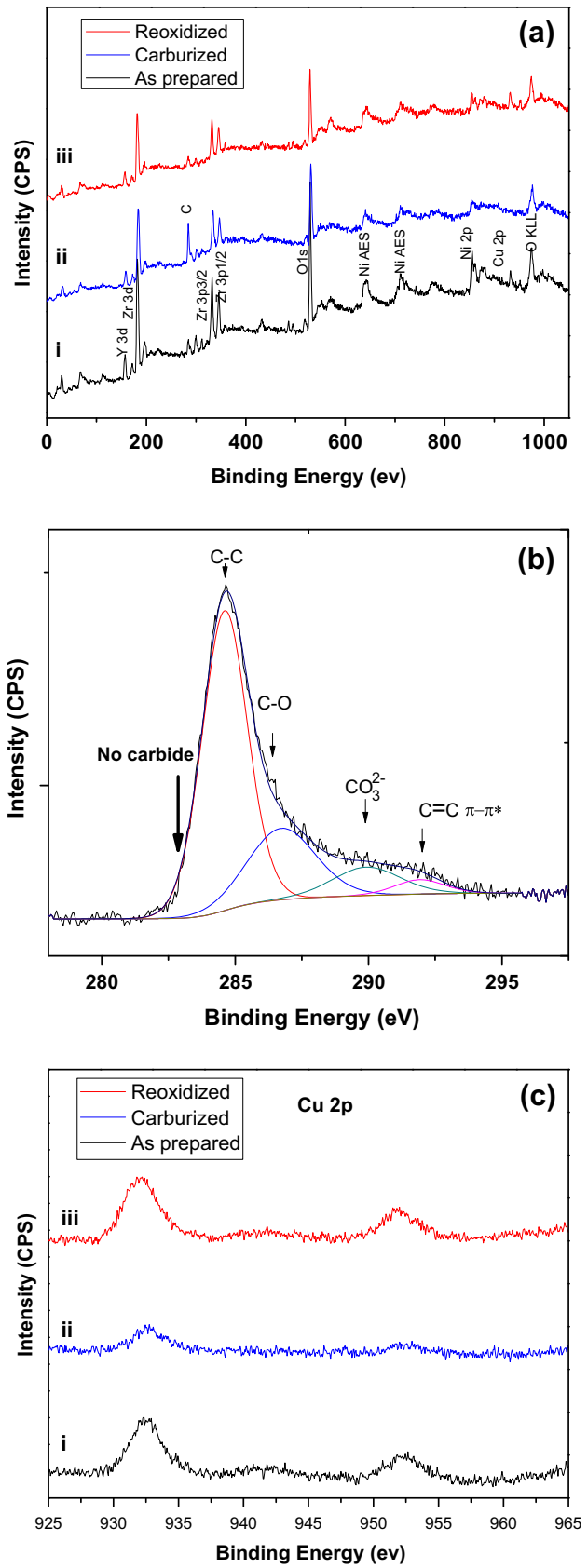

◀**Fig. 4** XPS spectra of **a** $Ni_{0.9}$–$Cu_{0.1}$–$YSZ_{0.95}$–$GDC_{0.05}$ anode **b** carbon peak of the carburized sample and **c** Cu2p peak (i. as-prepared, ii. carburized and iii. re-oxidized sample)

enrichment, a $Ni_{0.9}$–$Cu_{0.1}$–$YSZ_{0.95}$–$GDC_{0.05}$ anode-supported single cell, which was tested in methane fuel, was fractured and subjected to analysis. The line scan for Ni and Cu showed that there was a uniform distribution of bimetallic phase (Fig. 6) and no segregation of Cu was noticed.

Similarly, the line scan for C was carried out. It is interesting to note from Fig. 6b that there was no carbon deposition in most of the anode except at the electrolyte–anode and the anode–gas interface. In fact, carbon content in the electrolyte–anode interface was the highest with 12 wt%. The slight enrichment of carbon at the anode–gas interface is expected while cooling in OCV condition. But the presence of carbon near the electrolyte–anode interface shed some light on the reaction pathway. It suggested that methane cracking followed by electrochemical oxidation of carbon is the most likely pathway in the present case (Mogensen and Kammer 2003). The methane cracking mechanism involves three elementary steps (Eqs. 2–4).

$$C_xH_y \rightleftharpoons xC + y/2H_2 \quad (2)$$

$$C + 2O^{2-} \rightleftharpoons CO_2 + 4e^- \quad (3)$$

$$H_2 + O^{2-} \rightleftharpoons H_2O + 2e^- \quad (4)$$

The first step involves the cracking of methane into carbon and hydrogen followed by the oxidation of cracked products. In this process, the formation of carbon over catalyst surface is inevitable. Nevertheless, the anode catalyst should have the ability to oxidize the deposited carbon and resist the fiber formation. It was evident from Fig. 5d that there was not much change in anode microstructure after using methane fuel for 48 h. Thus, the absence of any carbon fiber in the anode confirmed that 9:1 Ni–Cu alloy is effective in reducing carbon deposits.

3.6 Electrochemical studies

3.6.1 Electrolyte-supported cell (ESC)

The merit of electrolyte-supported configuration (ESC) for studying the electrochemical parameters of the individual electrode is well established in the literature (Mcintosh et al. 2003). Therefore, 2-mm-thick ESC was fabricated and used for establishing the electrochemical parameters of the developed $Ni_{0.9}$–$Cu_{0.1}$–$YSZ_{0.95}$–$GDC_{0.05}$ anode in H_2 fuel (Fig. S6). The non-ohmic part of anode impedance was estimated from the difference between the low-frequency and high-frequency intercept. The impedance at

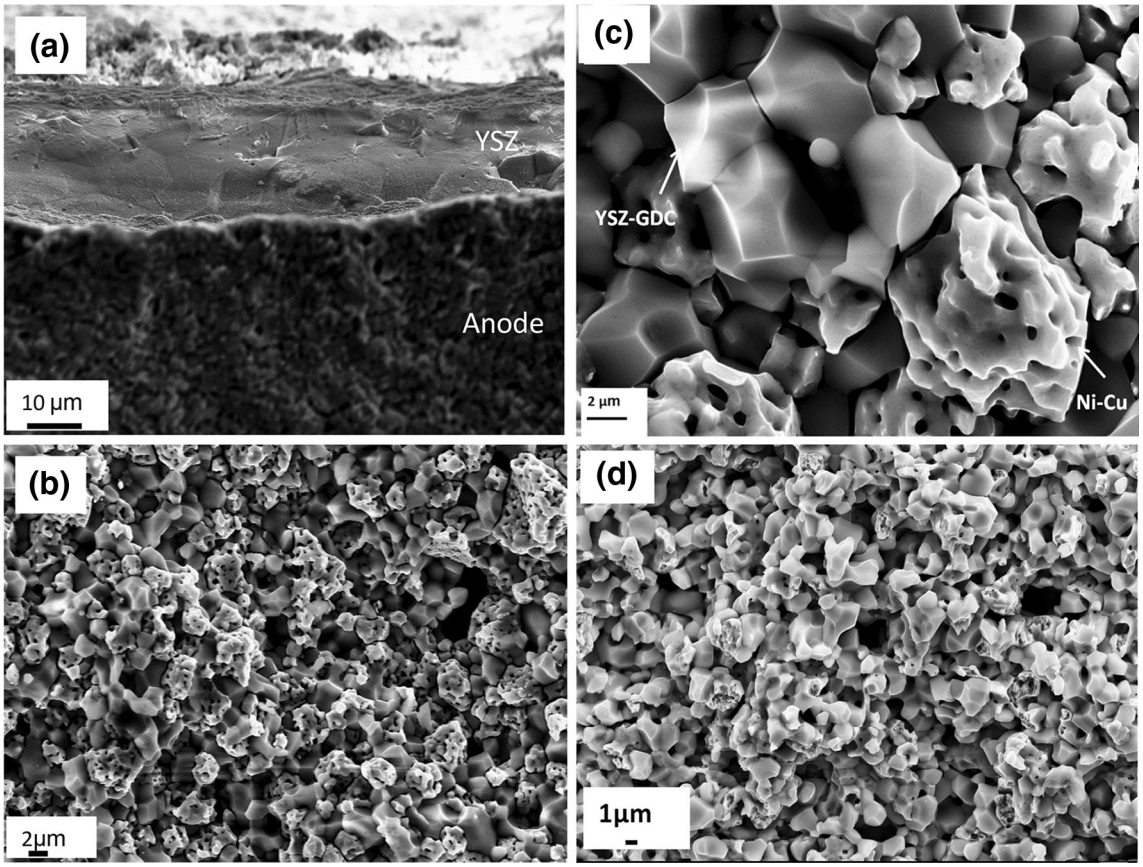

Fig. 5 FESEM images of **a** 8YSZ electrolyte on anode support, **b** $Ni_{0.9}$–$Cu_{0.1}$–$YSZ_{0.95}$–$GDC_{0.05}$ anode, **c** dense YSZ–GDC and porous Ni–Cu ensemble and **d** $Ni_{0.9}$–$Cu_{0.1}$–$YSZ_{0.95}$–$GDC_{0.05}$ anode after performing in CH_4 for 48 h

0.7 V was substantially lower than OCV (Fig. S7). Arrhenius plot generated with anode impedance is shown in Fig. 7a. The activation energy for anode kinetics was estimated from the slope of the Arrhenius plot. The activation energy (E_a) for $Ni_{0.9}$–$Cu_{0.1}$–$YSZ_{0.95}$–$GDC_{0.05}$ anode polarization was 1.01 eV which is comparable to the reported values of Ni–YSZ cermet (Leonide et al. 2009).

Exchange current density is another critical parameter, which was used to evaluate the performance of the electrocatalyst. It is a measure of the rate of electrochemical reaction at the reversible potential (OCV). There are many studies that used i_o to establish the electrocatalytic activity of anode (Grgicak et al. 2008; Vogler 2009). It is generally assumed in the past that the activation loss in SOFC is negligible and its dependent parameter, exchange current density, adds no weightage. The above assumption is valid only for high temperature SOFCs and tubular SOFCs because the activation loss becomes negligible at high operating temperatures ($\geq$ 1000 °C). Similarly, ohmic loss is substantially higher than activation loss in tubular designs. However, for the anode-supported planar cell, which operates at $\leq$ 800 °C with thin electrolyte, activation loss becomes significant and comparable with ohmic loss (Noren and Hoffman 2005). Hence, exchange current density is an important electrochemical property that measures the electrocatalytic activity of electrodes and it was calculated from the Tafel intercept at different temperatures (Fig. 7b) using ESC.

The estimated i_o of the developed anode increased from 20.9 mA cm^{-2} at 670 °C to 76.3 mA cm^{-2} at 780 °C. The E_a was found to be 1.03 eV. The close match between the activation energies derived from Arrhenius plots of anode polarization and exchange current density signifies the reasonable accuracy of i_o estimation. In general, it was believed that Cu addition affects the performance due to its material property and the stringent requirement for processing temperature (Grgicak et al. 2008). However, the high exchange current density indicated that $Ni_{0.90}$–$Cu_{0.10}$–$YSZ_{0.95}$–$GDC_{0.05}$ anode was able to overcome those constraints.

The performance comparison of the ESC in H_2 and CH_4 fuel was carried out (Fig. S8). The impedance analysis at OCV and 0.7 V indicated that faradic oxidation for methane was different from H_2. Further, it validates that CH_4 undergoes indirect oxidation reaction pathway as observed by EDAX analysis.

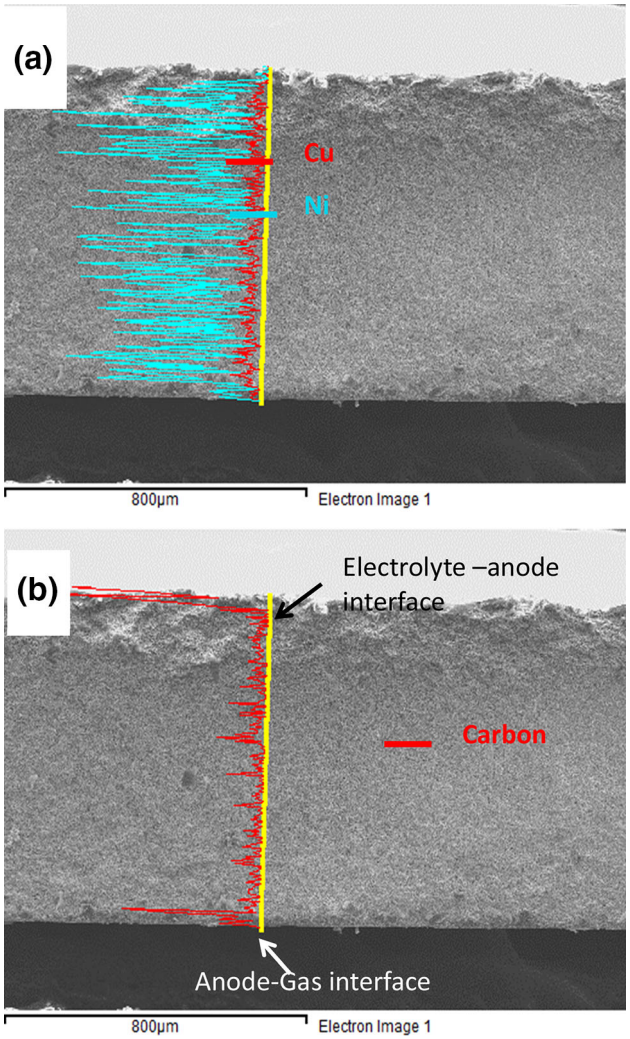

Fig. 6 Elemental mapping for **a** Ni–Cu and **b** carbon

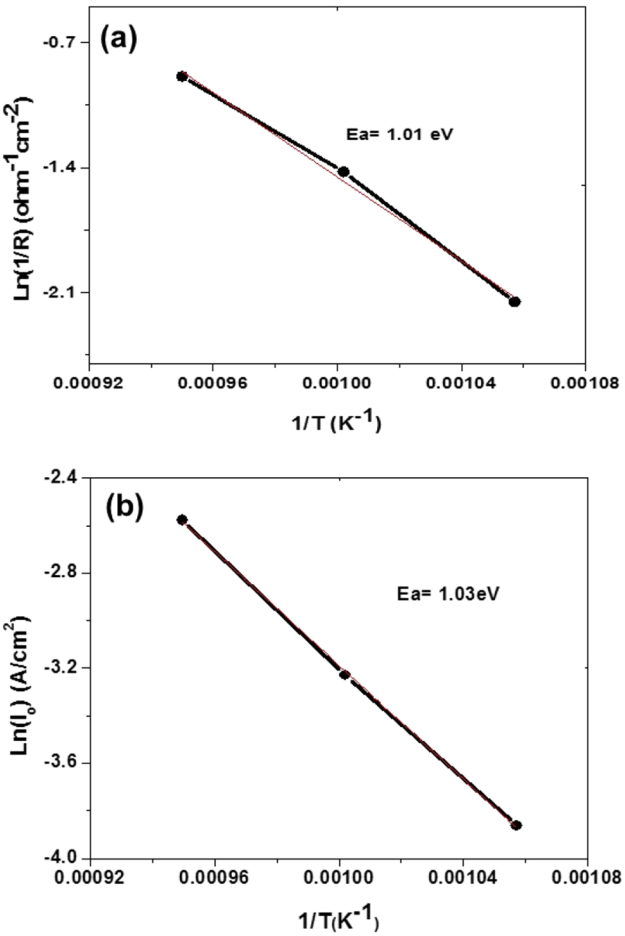

Fig. 7 Arrhenius plot of $Ni_{0.9}$–$Cu_{0.1}$–$YSZ_{0.95}$–$GDC_{0.05}$ anode **a** impedance and **b** exchange current density

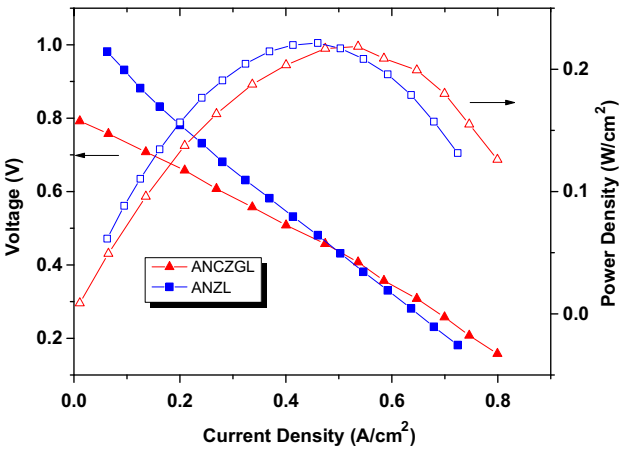

Fig. 8 Performance of filled square ANZL and filled triangle ANCZGL anode-supported single cells in H_2 fuel at 800 °C (filled and open symbol corresponds to voltage and power density, respectively)

3.6.2 Anode-supported cell (ASC)

The electrochemical performance curves of the ANCZGL and ANZL anode-supported cell in H_2 fuel are shown in Fig. 8. The maximum power density of ANCZGL was 219 mW cm^{-2} against 221 mW cm^{-2} of the ANZL at 800 °C. In fact, the area specific resistance (ASR) obtained from the slope of the *V–I* curve of the ANCZGL cell was 0.8 Ω cm^2 (Fig. S9), which was 30% lower than that of the standard Ni–YSZ-based cell.

The performance analysis of ANCZGL cell in methane was conducted in the temperature range of 707–824 °C (Fig. 9). There was a reduction in performance from 250 mW cm^{-2} at 824 °C to 56 mW cm^{-2} at 707 °C. The concentration polarization zone was distinctly visible with a limiting current density of ∼ 140 mA cm^{-2} at low temperatures. With the reduction in temperature, a reduced flux of oxide ion across the YSZ electrolyte would have led to some carbon deposition, which in turn would have constricted the gas diffusion. As methane cracking pathway results in carbon deposition, a good amount of oxygen flux is required to carry out the electrochemical oxidation of

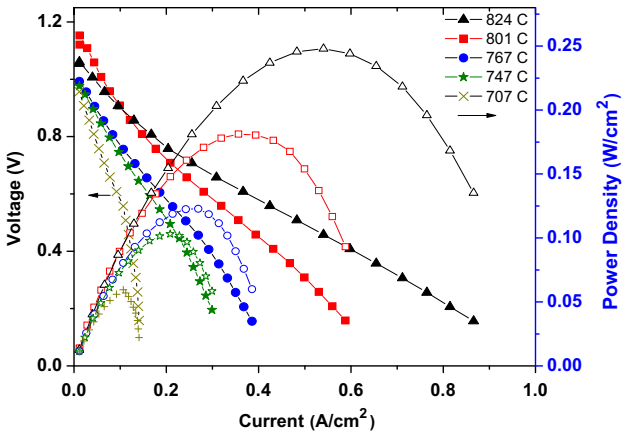

Fig. 9 Performance of anode-supported cell–ANCZGL in dry CH_4 fuel at (a) filled triangle 824 °C, (b) filled square 801 °C, (c) filled circle 767 °C, (d) asterisk 747 °C and (e) × 707 °C (filled and open symbol corresponds to voltage and power density, respectively)

deposited carbon. However, at operating temperature of ≥ 800 °C, there was no sign of concentration polarization. Hence, the possibility of such carbon deposition is low at high operating temperatures due to availability of sufficient oxygen flux.

The ASR of the cell calculated from the slope of polarization curve was 0.91 Ω cm^2 at 824 °C, which was lower than the value reported for Cu–CeO_2–YSZ system (Mcintosh et al. 2003). More specifically, the ASR was relatively lower at higher temperatures (≥ 800 °C). Since the cells were designed with YSZ electrolyte, operating temperature of 800 °C and above is required to ensure complete oxidation of fuel (Gorte et al. 2002). Accordingly, 800 °C is considered as the most favorable condition to suppress carbon deposition with the present anode system. As low- and high-temperature regions are dominated by Boudouard and methane cracking reactions, respectively (Sumi et al. 2011), carbon deposition was reduced at 800–850 °C, and hence, concentration polarization was absent in *V–I* plot (Fig. 9). In general, the anode system with high Cu content results in rapid Cu sintering at high operating temperature (Gross et al. 2007; Mcintosh et al. 2003). However, in the case of ANCZGL cell, the $Ni_{0.9}$–$Cu_{0.1}$–$YSZ_{0.95}$–$GDC_{0.05}$ anode prepared by the co-firing technique tends to form a perfect solid solution. So, the cells were operated comfortably ≥ 800 °C in methane for the entire experimental duration of 48 h.

The activation energy derived from total cell ASR versus 1/*T* plot of ANCZGL cell in methane was found to be 1.1 eV (Fig. S10), which was close to the activation energy for the process of oxygen ion conduction through the electrolyte. This implied that the oxygen ion conduction through the electrolyte could be the rate-limiting step for the anode reaction kinetics (Grgicak et al. 2008, Sumi et al. 2015). It was evident from the literature that the Ni–Cu–YSZ cermet had very high Ea of 177 kJ mol^{-1} (1.83 eV) in hydrocarbon fuel. The replacement of YSZ with ceria in the above anode drastically reduced the ASR by half (Muccillo et al. 2008). Accordingly, a wide range of ceria-based compositions have been reported in the literature (Park et al. 2000; Wang et al. 2008; Muccillo et al. 2008; La Rosa et al. 2007; Yano et al.; 2007; Zhang et al. 2002). However, ceria-rich compositions have been operated at low temperature (600–700 °C) to avoid phase stability issues. At low operating temperatures, the partial oxidation of fuel defeats the whole purpose of developing high efficiency systems (Mcintosh et al. 2003). With less than 2.5% GDC content, the developed $Ni_{0.90}$–$Cu_{0.10}$–$YSZ_{0.95}$–$GDC_{0.05}$ anode composition overcome the issues associated with the ceria and displayed good catalytic activity, carbon resistance and thermal stability at ≥ 800 °C.

The performance and electrochemical impedance (Fig. S11) analysis of ANCZGL cell in methane indicated that carbon deposition cannot be ruled out at low temperatures (< 750 °C). In order to understand the nature of such carbon deposit and its impact in performance, the ANCZGL cell was also tested in H_2 followed by 48 h testing in dry CH_4 fuel. Unlike the performance in methane, the slope I–V curve was almost constant in H_2 fuel at higher overpotentials (Fig. S12). The concentration polarization was not evident even at low temperature (707 °C) in H_2, and the maximum power density was 202 mW cm^{-2} in H_2 at 801 °C, which was ∼ 9% lower than initial performance. Hence, degradation of $Ni_{0.9}$-$Cu_{0.1}YSZ_{0.95}GDC_{0.05}$ in methane fuel was far less compared to reported Ni–YSZ (Mirzababaei and Chuang 2014; Woo et al. 2009), which degrades completely in 20 h. Moreover, the developed anode cermet had tendency to electrochemically oxidize the deposited carbon as a result the ANCZGL had stable performance in methane.

Given the fact that the present anode system uses lower Cu and minor GDC phases than the above systems, no degradation is expected for longer duration. Further, it is evident from the literature that 80:20 Cu–Ni ESC does not show any performance degradation in CH_4 up to 500 h (Kim et al. 2002). Also, Rosa et al. reported a stable performance (∼ 320 mA cm^{-2} at 0.6 V) up to 2000 h for ESC with $Ni_{0.6}$–$Cu_{0.4}$–GDC anode (La Rosa et al. 2007).

3.6.3 *Co-casted anode-supported cell*

In an attempt to improve the performance, co-casting of YSZ electrolyte was performed over the anode layer. The process was expected to improve the interaction of anode support and electrolyte and hence reduce the interface resistance. Accordingly, $Ni_{0.9}Cu_{0.1}$–$YSZ_{0.95}$–$GDC_{0.05}$ ASC (ANCZGC) was fabricated by utilizing bilayer electrolyte–anode, which was prepared by co-casting. The performance

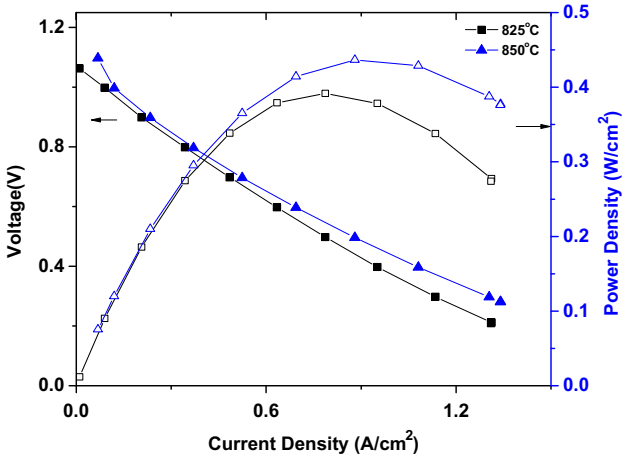

Fig. 10 Performance of anode-supported cell ANCZGC in CH_4 fuel at (a) filled triangle 850 °C, (b) filled square 825 °C (filled and open symbol corresponds to voltage and power density, respectively)

of ANCZGC is shown in Fig. 10. A maximum performance of 436 mW cm^{-2} was achieved at 850 °C for the cells tested in CH_4 fuel. The performance is relatively better than the similar SOFC anode compositions with Cu (Kim et al. 2002; Li et al. 2015; Mcintosh et al. 2003; Meng et al. 2013). The co-casting of YSZ electrolyte on the anode increased the performance of ANCZGC (392 mW cm^{-2}) over ANCZGL (248 mW cm^{-2}) by 58% at the operating temperature of $\sim$ 825 °C.

4 Conclusions

Attempt was made to develop high-performance anode-supported SOFC suitable for hydrocarbon fuel. In the present work, the Cu and GDC content was optimized to realize the $Ni_{0.9}Cu_{0.1}YSZ_{0.95}GDC_{0.05}$ anode composite, which had better thermal stability toward fabrication conditions, reasonable electrical conductivity, good electrocatalytic activity and excellent resistance for carbon deposition. The carburization studies showed that $Ni_{0.9}$–$Cu_{0.1}$–$YSZ_{0.95}$–$GDC_{0.05}$ composition had tendency to reduce the carbon deposition up to 50%. Also, the developed composition withstood the high temperature in the typical co-firing process of anode-supported cell fabrication. The electrical characterization revealed that $Ni_{0.9}$-$Cu_{0.1}$–$YSZ_{0.95}$–$GDC_{0.05}$ composite anode exhibited an electrical conductivity 846 S cm^{-1}, which is reasonably good for SOFC anode. The work demonstrated that anode can be utilized in ESC and ASC configurations. The electrochemical parameters such as anode impedance and exchange current densities were estimated and found to be par with standard Ni–YSZ in H_2 fuel. The ASC with laminated layers of electrolyte and anode was operated in methane. The laminated cell had performed impressively in the temperature range of 800–850 °C with low ASR and lasted for entire experimental duration without much degradation. The post-methane analysis revealed that the developed anode cermet had tendency to electrochemically oxidize the deposited carbon. Similarly, the developed co-cast ASC had a highest power density of 436 mW cm^{-2} at 850 °C and 0.5 V in methane fuel. The results were consistent and reproducible in several cells. Thus, the present anode is a promising one as it possesses the required carbon tolerance, catalytic activity and reasonable power density in hydrocarbon fuel. The feasibility of fabrication of thermally sensitive Ni–Cu anode composition without compromising the electrocatalytic activity has been shown in this study, and the developed new anode composition and fabrication routes employed may act as a precedent to evolve high power density SOFCs for hydrocarbon fuels.

Acknowledgements The authors express their sincere gratitude to the Director, NAL and Head, SED, for their constant support and encouragement. The authors acknowledge the help received from Dr. P. Bera, Mr.G. Srinivas and Mr. Siju in XPS, XRD and FESEM, respectively.

References

Ahn K, He H, Vohs JM, Gorte RJ (2005) Enhanced thermal stability of SOFC anodes made with CeO_2–ZrO_2 solutions. Electrochem Solid-State Lett 8:A414–A417. https://doi.org/10.1149/1.1945374

Bayer BC, Bosworth DA, Michaelis FB, Blume R, Habler G, Abart R (2016) In situ observations of phase transitions in metastable nickel (carbide)/carbon nanocomposites. J Phys Chem C 120:22571–22584. https://doi.org/10.1021/acs.jpcc.6b01555

Cabrera ER, Atkinson A, Chadwick D (2004) Catalytic steam reforming of methane over $Ce_{0.9}Gd_{0.1}O_{2-x}$. Appl Catal B Environ 47:127–131. https://doi.org/10.1016/j.apcatb.2003.08.008

Camacho LFDE, Vivas JAM (2009) Copper–terbia and copper–gadolina anodes for direct hydrocarbon solid oxide fuel cells: A fundamental comparison of their physicochemical features and performances. Fuel 88:1970–1974. https://doi.org/10.1016/j.fuel.2009.03.019

Campbell CT, Peden CHF (2004) Chemistry. Oxygen vacancies and catalysis on ceria surfaces. Science 309(5735):713–714

Chun CM, Ramanarayanan TA (2007) Mechanism and control of carbon deposition on high temperature alloys. J Electrochem Soc 154(9):C465–C471. https://doi.org/10.1149/1.2750447

Constantin G, Rossignol C, Briois P, Billard A, Dessemond L (2012) Influence of gadolinia-doped ceria buffer layer on the durability of LSCF/CGO/YSZ system for IT-SOFC. J Electrochem Soc 45:295–305. https://doi.org/10.1149/1.3701319

Eric H, Timu M (1979) Equilibrium relations in the system nickel oxide-copper oxide. Metall Trans B 10:561–563. https://doi.org/10.1007/BF02662558

Esconjauregui S, Whelan CM, Maex K (2009) The reasons why metals catalyze the nucleation and growth of carbon nanotubes

and other carbon nanomorphologies. Carbon 47:659–669. https://doi.org/10.1016/j.carbon.2008.10.047

Fuerte A, Valenzuela RX, Escudero MJ, Daza L (2011) Effect of cobalt incorporation in copper-ceria based anodes for hydrocarbon utilisation in Intermediate temperature solid oxide fuel cells. J Power Sources 196:4324–4331. https://doi.org/10.1016/j.jpowsour.2010.12.053

Gorte RJ, Kim H, Vohs JM (2002) Novel SOFC anodes for the direct electrochemical oxidation of hydrocarbon. J Power Sources 106:10–15. https://doi.org/10.1016/S0378-7753(01)01021-7

Grgicak CM, Pakulska MM, Brien JSO, Giorgi JB (2008) Synergistic effects of $Ni_{1-x}Co_x$-YSZ and $Ni_{1-x}Cu_x$-YSZ alloyed cermet SOFC anodes for oxidation of hydrogen and methane fuels containing H2S. J Power Sources 183:26–33. https://doi.org/10.1016/j.jpowsour.2008.05.002

Gross MD, Vohs JM, Gorte RJ (2007) A study of thermal stability and methane tolerance of Cu-based SOFC anodes with electrodeposited Co. Electrochim Acta 52:1951–1957. https://doi.org/10.1016/j.electacta.2006.08.005

Gupta GK, Dean AM, Ahn K, Gorte RJ (2006) Show more comparison of conversion and deposit formation of ethanol and butane under SOFC conditions. J Power Sources 158:497–503. https://doi.org/10.1016/j.jpowsour.2005.09.036

Iida T, Kawano M, Matsui T, Kikuchi R, Eguchi K (2007) Internal reforming of SOFCs carbon deposition on fuel electrode and subsequent deterioration of cell. J Electrochem Soc 154:B234–B241. https://doi.org/10.1149/1.2405837

Ingram DB, Linic S (2009) First-principles analysis of the activity of transition and noble metals in the direct utilization of hydrocarbon fuels at solid oxide fuel cell operating conditions. J Electrochem Soc 156:B1457–B1465. https://doi.org/10.1149/1.3240101

Kaur G, Basu S (2013) Performance studies of copper–iron/ceria–yttria stabilized zirconia anode for electro-oxidation of butane in solid oxide fuel cells. J Power Sources 241:783–790. https://doi.org/10.1016/j.jpowsour.2013.02.083

Kharlamova MV (2017) Investigation of growth dynamics of carbon nanotubes. Beilstein J Nanotechnol 8:826–856. https://doi.org/10.3762/bjnano.8.85

Kim H, Lu C, Worrell WL, Vohs JM, Gorte RJ (2002) Cu–Ni cermet anodes for direct oxidation of methane in solid-oxide fuel cells. J Electrochem Soc 149:A247–A250. https://doi.org/10.1149/1.1445170

Kim T, Ahn K, Vohs JM, Gorte RJ (2007) Deactivation of ceria-based SOFC anodes in methanol. J Power Sources 164:42–48. https://doi.org/10.1016/j.jpowsour.2006.09.101

Kim G, Corre G, Irvine JTS, Vohs JM, Gorte RJ (2008) Engineering composite oxide SOFC anodes for efficient oxidation of methane. Electrochem Solid State Lett 11:B16–B19. https://doi.org/10.1149/1.2817809

Kim G, Lee S, Shin JY, Corre G, Irvine JTS, Vohs JM, Gorte RJ (2009) Investigation of the structural and catalytic requirements for high-performance SOFC anodes formed by infiltration of LSCM. Electrochem Solid-State Lett 12:B48–B52. https://doi.org/10.1149/1.3065971

La Rosa D, Faro ML, Monforte G, Antonucci V, Aricò AS, Sin A (2007) Recent advances on the development of NiCu alloy catalysts for IT-SOFCs. ECS Trans 7:1685–1693. https://doi.org/10.1149/1.2729278

Leonide A, Apel Y, Ivers-Tiffée E (2009) SOFC modeling and parameter identification by means of impedance spectroscopy. ECS Trans 19:81–109. https://doi.org/10.1149/1.3247567

Li M, Hua B, Pu J, Chi B, Jian L (2015) Electrochemical performance and carbon deposition resistance of M-$BaZr_{0.1}Ce_{0.7}Y_{0.1}$ $Yb_{0.1}$-$O_{3-\delta}$ (M = Pd, Cu, Ni or NiCu) anodes for solid oxide fuel cells. Sci Rep 5(7667):1–7. https://doi.org/10.1038/srep07667

Lu XC, Zhu JH, Bi ZH (2009) Fe alloying effect on the performance of the Ni anode in hydrogen fuel. Solid State Ionics 180:265–270. https://doi.org/10.1016/j.ssi.2008.12.011

Ma Q, Tietz F, Sebold D, Stöver D (2010) Y-substituted $SrTiO_3$–YSZ composites as anode materials for solid oxide fuel cells: interaction between SYT and YSZ. J Power Sources 195:1920–1925. https://doi.org/10.1016/j.jpowsour.2009.09.075

Ma Q, Tietz F, Stöver D (2011a) Nonstoichiometric Y-substituted $SrTiO_3$ materials as anodes for solid oxide fuel cells. Solid State Ion 192:535–539. https://doi.org/10.1016/j.ssi.2010.03.027

Ma Q, Tietz F, Leonide A, Ivers-Tiffee E (2011b) Electrochemical performances of solid oxide fuel cells based on Y-substituted $SrTiO_3$ ceramic anode materials. J Power Sources 196:7308–7312. https://doi.org/10.1016/j.jpowsour.2010.07.094

Mcintosh S, Vohs JM, Gorte RJ (2003) Impedance spectroscopy for the characterization of Cu-Ceria-YSZ anodes for SOFCs. J Electrochem Soc 150:A1305–A1312. https://doi.org/10.1149/1.1603246

Meng XX, Gong X, Yang NT, Tan XY, Ma ZF, Xuebao WH (2013) Preparation and properties of direct-methane solid oxide fuel cell based on a graded Cu–CeO_2–Ni-YSZ composite anode. Acta Phys Chim Sin 29:1719–1726. https://doi.org/10.3866/PKU.WHXB201305151

Mirzababaei J, Chuang SSC (2014) $La_{0.6}Sr_{0.4}Co_{0.2}Fe_{0.8}O_3$ perovskite: a stable anode catalyst for direct methane solid oxide fuel cells. Catalysts 4:146. https://doi.org/10.3390/catal4020146

Mishima Y, Mitsuyasu H, Ohtaki M, Eguchi K (1998) Solid oxide fuel cell with composite electrolyte consisting of samaria-doped ceria and yttria-stabilized zirconia. J Electrochem Soc 145:1004–1007. https://doi.org/10.1149/1.1838378

Mogensen M, Kammer K (2003) Conversion of hydrocarbons in solid oxide fuel cells. Annu Rev Mater Res 33:321–331. https://doi.org/10.1146/annurev.matsci.33.022802.092713

Muccillo R, Muccillo ENS, Fonseca FC, Florio DZD (2008) Characteristics and performance of electrolyte-supported solid oxide fuel cells under ethanol and hydrogen. J Electrochem Soc 155:B232–B235. https://doi.org/10.1149/1.2828024

Murray EP, Tsai T, Barnett SA (1999) A direct-methane fuel cell with a ceria-based anode. Nature 400:649–651. https://doi.org/10.1038/23220

Neofytidis C, Dracopoulos V, Neophytides SG, Niakolas DK (2018) Electrocatalytic performance and carbon tolerance of ternary Au–Mo–Ni/GDC SOFC anodes under CH_4-rich internal steam reforming conditions. Catal Today 310:157–165. https://doi.org/10.1016/j.cattod.2017.06.028

Noren DA, Hoffman MA (2005) Clarifying the Butler–Volmer equation and related approximations for calculating activation losses in solid oxide fuel cell models. J Power Sources 152:175–181. https://doi.org/10.1016/j.jpowsour.2005.03.174

Palaniyandi V, Shamsuzzoha M, Ada ET, Zangari G, Reddy RG (2006) Microstructural evolution of nickel nanoparticle catalysts supported on gadolinium-doped ceria during autothermal reforming of iso-octane. J Electron Mater 35:814–821. https://doi.org/10.1007/BF02692534

Park S, Vohs JM, Gorte RJ (2000) Direct oxidation of hydrocarbons in a solid-oxide fuel cell. Nature 404:265–267. https://doi.org/10.1038/35005040

Patil KC, Aruna ST, Mimani T (2002) Combustion synthesis: an update. Curr Opin Solid State Mater Sci 6:507–512. https://doi.org/10.1016/S1359-0286(02)00123-7

Prakash BS, Kumar SS, Aruna ST (2017) Effect of composition on the polarization and ohmic resistances of LSM/YSZ composite cathodes in solid oxide fuel cell. Bull Mater Sci 40:441–452. https://doi.org/10.1007/s12034-017-1401-5

Rao R, Sharma R, Abild-Pedersen F, Nørskov JK, Harutyunyan AR (2014) Insights into carbon nanotube nucleation: cap formation

governed by catalyst interfacial step flow. Sci Rep 4(6510):1–6. https://doi.org/10.1038/srep06510

Rodriguez NM, Kim MS, Baker RTK (1993) Deactivation of copper nickel-catalysts due to changes in surface composition. J Catal 140:16–29. https://doi.org/10.1006/jcat.1993.1065

Rührup V, Wiemhöfer HD, Naturforsch Z (2006) Ionic conductivity of Gd-and Y-doped ceria-zirconia solid solutions. Adv J Chem Sci 61(7):916–922. https://doi.org/10.1515/znb-2006-0721

Rupp JLM, Infortuna A, Gauckler LJ (2007) Thermodynamic stability of gadolinia-doped ceria thin film electrolytes for micro-solid oxide fuel cells. J Am Ceram Soc 90:1792–1797. https://doi.org/10.1111/j.1551-2916.2007.01531.x

Sarno C, Luisetto I, Zurlo F, Licoccia S, Bartolomeo ED (2018) Lanthanum chromite based composite anodes for dry reforming of methane. Int J Hydrog Energy 43(31):14742–14750. https://doi.org/10.1016/j.ijhydene.2018.06.021

Shiratori Y, Oshima T, Sasaki K (2008) Feasibility of direct-biogas SOFC. Int J Hydrog Energy 33:6316–6321. https://doi.org/10.1016/j.ijhydene.2008.07.101

Simwonis D, Tietz F, Stöver D (2000) Nickel coarsening in annealed Ni/8YSZ anode substrates for solid oxide fuel cells. Solid State Ion 132:241–251. https://doi.org/10.1016/S0167-2738(00)00650-0

Sumi H, Lee YH, Muroyama H, Matsui T, Kamijo M, Mimuro S, Yamanaka M, Nakajima Y, Eguchi K (2011) Effect of carbon deposition by carbon monoxide disproportionation on electrochemical characteristics at low temperature operation for solid oxide fuel cells. J Power Sources 196:4451–4457. https://doi.org/10.1016/j.jpowsour.2011.01.061

Sumi H, Shimada H, Yamaguchi T, Hamamoto K, Suzuki T, Fujishiro Y (2015) Development of microtubular solid oxide fuel cells using hydrocarbon fuels. In: Bansal NP, Kusnezoff M, Shimamura K (eds) Advances in solid oxide fuel cells and electronic ceramics, vol 599. Wiley, New York, pp 1–3. https://doi.org/10.1002/9781119211501

Sun C, Su R, Chen J, Lu L, Guan P (2019) Carbon formation mechanism of C_2H_2 in Ni-based catalysts revealed by in situ electron microscopy and molecular dynamics simulations. ACS Omega 4:8413–8420. https://doi.org/10.1021/acsomega.9b00958

Vogler M (2009) Thesis: elementary kinetic modelling applied to solid oxide fuel cell pattern anode and a direct flame fuel cell system. Heidelberg University Publishing, Płock, p 33

Wang Z, Weng W, Cheng K, Du P, Shen G, Han G (2008) Catalytic modification of Ni–Sm-doped ceria anodes with copper for direct utilization of dry methane in low-temperature solid oxide fuel cells. J Power Sources 179:541–546. https://doi.org/10.1016/j.jpowsour.2008.01.040

Woo E, Moon H, Park M, Hoon S (2009) Fabrication and characterization of Cu–Ni–YSZ SOFC anodes for direct use of methane via Cu-electroplating. Int J Hydrog Energy 34:5537–5545. https://doi.org/10.1016/j.ijhydene.2009.04.060

Wu C, Wu F, Bai Y, Liu Y, Sun J (2007) Hydrogen Generation from ethanol steam reforming over rare earth promoted nickel-based catalysts. IEEE. https://doi.org/10.1109/ICCA.2007.4376484

Yano M, Kawai T, Okamoto K, Nagao M, Sano M, Tomita A, Hibino T (2007) Single-chamber SOFCs using dimethyl ether and ethanol. J Electrochem Soc 8:B865–B870. https://doi.org/10.1149/1.2747326

Yu F, Xia J, Zhang Y, Weizi C, Xie Y, Yang N, Liu J, Liu M (2019) New insights into carbon deposition mechanism of nickel/yttrium-stabilized zirconia cermet from methane by in situ investigation. Appl Energy 256:113910. https://doi.org/10.1016/j.apenergy.2019.113910

Zhang X, Ohara S, Chen H, Fukui T (2002) Conversion of methane to syngas in a solid oxide fuel cell with Ni–SDC anode and LSGM electrolyte. Fuel 81:989–996. https://doi.org/10.1016/S0016-2361(02)00012-1

Zhao L, Ye X, Zhan Z (2011) High-performance cathode-supported solid oxide fuel cells with copper cermet anodes. J Power Sources 196:6201–6204. https://doi.org/10.1016/j.jpowsour.2011.03.091

Zhao K, Hou X, Norton MG, Ha S (2019) Application of a NiMo–$Ce_{0.5}Zr_{0.5}O_{2-\delta}$ catalyst for solid oxide fuel cells running on gasoline. J Power Sources 435:226732. https://doi.org/10.1016/j.jpowsour.2019.226732

Zhou W, Shao Z, Liang F, Chen ZG, Zhu Z, Jin W, Xu N (2011) A new cathode for solid oxide fuel cells capable of in situ electrochemical regeneration. J Mater Chem 21:15343–15351. https://doi.org/10.1039/C1JM12660A